A Multiple-Antenna System for ISM Band Transmission - Calibration Issues and Eigenbeam Measurements

Mark Petermann, Henning Paul, Dirk Wübben, Karl-Dirk Kammeyer
Department of Communications Engineering
University of Bremen, 28359 Bremen, Germany
Email: {petermann, paul, wuebben, kammeyer}@ant.uni-bremen.de

***Abstract*— In this paper, we present eigenbeam measurements performed with our multiple-antenna demonstrator MASI. The existing angle offset of the estimated eigenbeams motivated calibration and verification measurements in an anechoic chamber. After eliminating the sources of errors via phase calibration this squinting is removed and the estimated direction-of-arrivals of the transmit signal become plausible. Additional measurements of a rotating receive array sustain the successful off-line phase calibration.**

***Index Terms*— MIMO, MASI, RF Impairments, Calibration, Eigenbeams, DOA Estimation**

I. Introduction

Multiple-Input Multiple-Output (MIMO) systems are essential to fulfill the growing demands of data rate and reliability in wireless communications without increasing the required bandwidth. This also holds for modern and future communication systems, which use Orthogonal Frequency Division Multiplexing (OFDM) as common air interface [1]. Designated schemes like the Bell Labs Layered Space Time (BLAST) architecture or precoding and beamforming techniques not only cause higher effort to be spent on signal processing but also make high demands on hardware components with respect to quality and tolerance. As each additional antenna element needs a separate front-end with individual components, conditional of manufacturing, the relative gain and phasing of the transmit (Tx) and receive (Rx) signals are influenced by several radio frequency (RF) impairments.

This also holds for our multiple-antenna demonstrator called MASI (**M**ultiple-**A**ntenna **S**ystem for **I**SM Band Transmission), originally introduced in [2]. With it, a verification of simulation results in a real transmission with general impairments like synchronisation and timing aspects is possible. Unfortunately, the employed hardware components inherently cause different circuitry characteristics in each Tx and Rx path. These characteristics need to be accounted for with calibration approaches, which can be either done with an external reference source or relative and absolute calibration [3]. Here, we consider the latter. The need for calibration was shown in [4], where measurements of the channel eigenbeams, which indicate preferred directions of the emitted electromagnetic waves, produced a permanent beam-squint of the main lobe in a magnitude of several degrees.

Hence, this contribution deals with the calibration and measurement campaign conducted in our institute to combat this squinting and to identify the preferred directions of the eigenbeams [5]. Afterwards, also the number of propagating modes of the (estimated) channel can be identified in line-of-sight (LOS) and non-LOS (NLOS) scenarios.

The remainder of the paper is organized as follows. Section II introduces the applicable MIMO array system model and the necessary basics about the array factor of eigenbeams. In Section III the interfering hardware components are illustrated in more detail. Subsequently, Section IV describes the calibration and verification approach. Measurement results are shown in Section V and a conclusion in Section VI completes the paper.

II. MIMO Array System Model

We assume a MIMO system with N_{T} omnidirectional transmit and N_{R} omnidirectional receive antennas. Both antenna arrays are arranged as uniform linear arrays (ULAs), where the antenna spacing is d. For both the Tx and the Rx array the elements of the so-called steering vectors $\mathbf{b}(\theta) \in \mathbb{C}^{N_{\mathrm{T}}}$ and $\mathbf{a}(\theta) \in \mathbb{C}^{N_{\mathrm{R}}}$ (assuming zero elevation) can be described as

$$b_k(\theta) = \exp\left(j\frac{2\pi}{\lambda_{\mathrm{c}}} d(k-1)\sin(\theta) \right) \qquad (1)$$

$$a_i(\theta) = \exp\left(-j\frac{2\pi}{\lambda_{\mathrm{c}}} d(i-1)\sin(\theta) \right). \qquad (2)$$

This work was supported in part by the German Research Foundation (DFG) under grant Ka841-21/1.

Here, $\lambda_c = c_0/f_c$, where c_0 is the speed of light and f_c denotes the carrier frequency of the coplanar signals. Then the steering vectors describe the phase available at an antenna element relative to a reference antenna element depending on the azimuth angle $\theta \in [0°, 360°)$. Information about a steering vector $\mathbf{b}(\theta_\ell)$ or $\mathbf{a}(\theta_\ell)$, where θ_ℓ denotes the azimuth angle for a specific signal path ℓ, is critical in finding the directions-of-arrival (DOAs) and directions-of-departure (DODs) or in applying space processing algorithms like beamforming [6].

Thus, the baseband continuous-time signal at the receiver with path delays τ_ℓ at time instant t can be expressed as in (3), where $\mathbf{y}(t, \tau_\ell) \in \mathbb{C}^{N_R}$, $\mathbf{x}(t) \in \mathbb{C}^{N_T}$ and $\mathbf{n}(t) \in \mathbb{C}^{N_R}$ denote the complex receive vector, transmit vector and white Gaussian noise vector, respectively. $g_\ell(t - \tau_\ell)$ represents the complex path coefficient and L is the maximum number of independent signal paths. $(\cdot)^T$ corresponds to the transposition of a vector.

The bandwidth of the transmitted signals shall be small compared to the carrier frequency f_c. This narrowband assumption guarantees that the signals are received with practically the same phase at the antenna elements. Small differences in delay τ_ℓ can be ingnored, since they are small compared to the channel coherence time. With it, the complex channel matrix at a certain time instance t can be written as

$$\mathbf{H}(t) = \sum_{\ell=1}^{L} \mathbf{a}(\theta_\ell, t)\, g_\ell(t)\, \mathbf{b}(\theta_\ell, t)^T \in \mathbb{C}^{N_R \times N_T}. \quad (4)$$

The Tx and Rx autocorrelation matrices and their corresponding eigenvalue decompositions are defined as [5]

$$\mathbf{R}_{\mathbf{H}}^{(\mathrm{Tx})} = \mathrm{E}\left\{ \mathbf{H}(t)^H \mathbf{H}(t) \right\} = \mathbf{H}^H \mathbf{H} = \mathbf{V}_T \mathbf{\Lambda}_T \mathbf{V}_T^H \quad (5)$$

$$\mathbf{R}_{\mathbf{H}}^{(\mathrm{Rx})} = \mathrm{E}\left\{ \mathbf{H}(t)\, \mathbf{H}(t)^H \right\} = \mathbf{H}\mathbf{H}^H = \mathbf{V}_R \mathbf{\Lambda}_R \mathbf{V}_R^H, \quad (6)$$

where time index t can be omitted due to the assumed static scenario. Then, $\mathbf{H}$ is the flat channel matrix per frame, which needs to be estimated at the receiver. Here, $(\cdot)^H$ denotes the Hermitian transpose of a matrix. With (5) and (6) the Tx and Rx eigenbeam array factors can be obtained via

$$f_{T,k}(\theta) = \mathbf{v}_{T,k}^H \mathbf{b}(\theta) \quad \text{and} \quad f_{R,i}(\theta) = \mathbf{v}_{R,i}^H \mathbf{a}(\theta), \quad (7)$$

where $\mathbf{v}_{T,k}$ is the k-th column of $\mathbf{V}_T$, etc. For illustration purposes we normalized the array factor in (7) to the power of the corresponding eigenvalue.

III. Hardware Influences

The MIMO demonstrator MASI presented in [2] is a very flexible low cost direct-conversion measurement system. It operates in the license-free 2.4 GHz ISM band and allows for directly storing generated I/Q data samples in a digital Tx buffer via an USB interface. These samples in a frame are adressed in a circular manner. The currently addressed frame is fed to the digital-to-analog converters (DAC), whose baseband outputs pass the RF stage, which up-converts the signal into the desired RF frequency band. At the transmitter and the receiver the intended modular architecture implies that each antenna plug-in module is provided by a central clock for the digital clock as well as for the local oscillators (LO). This configuration as shown in Fig. 1 ensures that inter-module synchronisation of sample rate and carrier phase is possible. Unfortunately, the same LO

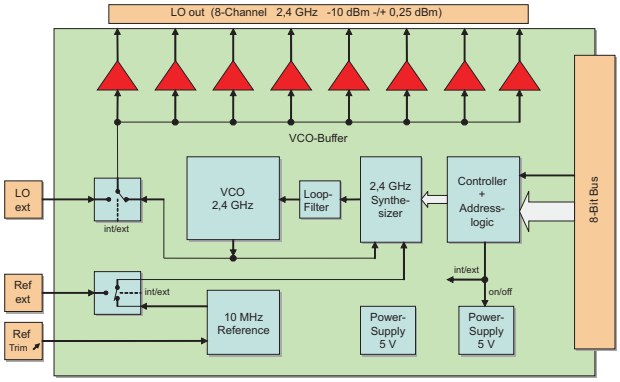

Fig. 1. Schematic of the MASI local oscillator and splitter configuration

signal cannot be provided at the antennas after the LO stage as different amplifiers are present in each antenna branch (see *red* elements in Fig. 1). This suboptimal LO signal distribution leads to relative phase offsets after passing through the devices due to the existing tolerance of the employed components. Thus, the assumed narrowband equal phase signal situation is no longer existent as all antenna signals have different phases afterwards.

The occurring phase distortions at the transmitter and the receiver can be modeled as diagonal filter

$$\mathbf{y}(t, \tau_\ell) = \sum_{\ell=1}^{L} \mathbf{a}(\theta_\ell, t)\, g_\ell(t - \tau_\ell)\, \mathbf{b}(\theta_\ell, t)^T \mathbf{x}(t) + \mathbf{n}(t) \quad (3)$$

matrices $\mathbf{\Phi}_{\mathrm{T}}$=diag$\{[\exp(j\phi_{\mathrm{T},1}),\ldots,\exp(j\phi_{\mathrm{T},N_{\mathrm{T}}})]\}$ and $\mathbf{\Phi}_{\mathrm{R}} = \mathrm{diag}\{[\exp(j\phi_{\mathrm{R},1}),\ldots,\exp(j\phi_{\mathrm{R},N_{\mathrm{R}}})]\}$, where the $\mathrm{diag}\{\cdot\}$-operator assigns the elements of a vector on the main diagonal of a matrix. The phase distortion of the LO amplifier at an antenna module is described by $\phi_{\mathrm{T},k}$ at the transmitter and $\phi_{\mathrm{R},i}$ at the receiver. Consequently, the overall channel matrix including the LO path imperfections can be written to

$$\tilde{\mathbf{H}} = \mathbf{\Phi}_{\mathrm{R}}\mathbf{H}\mathbf{\Phi}_{\mathrm{T}} \ . \tag{8}$$

This in turn affects the transmit and receive auto-correlation matrices of the overall channel such that $\mathbf{R}_{\tilde{\mathbf{H}}}^{(\mathrm{Tx})}$ becomes

$$\begin{aligned}\mathbf{R}_{\tilde{\mathbf{H}}}^{(\mathrm{Tx})} &= \tilde{\mathbf{H}}^H\tilde{\mathbf{H}} = \mathbf{\Phi}_{\mathrm{T}}^H\mathbf{H}^H\mathbf{\Phi}_{\mathrm{R}}^H\mathbf{\Phi}_{\mathrm{R}}\mathbf{H}\mathbf{\Phi}_{\mathrm{T}} \\ &= \mathbf{\Phi}_{\mathrm{T}}^H\mathbf{R}_{\mathbf{H}}^{(\mathrm{Tx})}\mathbf{\Phi}_{\mathrm{T}} = \tilde{\mathbf{V}}_{\mathrm{T}}\mathbf{\Lambda}_{\mathrm{T}}\tilde{\mathbf{V}}_{\mathrm{T}}^H\end{aligned} \tag{9}$$

with $\tilde{\mathbf{V}}_{\mathrm{T}} = \mathbf{\Phi}_{\mathrm{T}}^H\mathbf{V}_{\mathrm{T}}$ and likewise $\mathbf{R}_{\tilde{\mathbf{H}}}^{(\mathrm{Rx})}$ becomes

$$\mathbf{R}_{\tilde{\mathbf{H}}}^{(\mathrm{Rx})} = \tilde{\mathbf{H}}\tilde{\mathbf{H}}^H = \mathbf{\Phi}_{\mathrm{R}}\mathbf{R}_{\mathbf{H}}^{(\mathrm{Rx})}\mathbf{\Phi}_{\mathrm{R}}^H = \tilde{\mathbf{V}}_{\mathrm{R}}\mathbf{\Lambda}_{\mathrm{R}}\tilde{\mathbf{V}}_{\mathrm{R}}^H \tag{10}$$

with $\tilde{\mathbf{V}}_{\mathrm{R}} = \mathbf{\Phi}_{\mathrm{R}}\mathbf{V}_{\mathrm{R}}$. Notice that contrary to $\tilde{\mathbf{V}}_{\mathrm{T}}$ and $\tilde{\mathbf{V}}_{\mathrm{R}}$ the matrices of eigenvalues $\mathbf{\Lambda}_{\mathrm{T}}$ and $\mathbf{\Lambda}_{\mathrm{R}}$ are the same as in (5) and (6). However, as the eigenvectors are used to obtain the array factors of the Tx and Rx arrays in (7), this difference explains the squinting of the beams.

It is worth to be mentioned that the results obtained, e.g., in [7], [8] are not affected by the phase errors as conventional channel estimation algorithms are used to obtain $\tilde{\mathbf{H}}$ at the receiver. Hence, the phases are incorporated in additional space-time processing algorithms based on $\tilde{\mathbf{H}}$.

IV. Calibration

Since locating the occuring phase differences in the LO paths was not apparent at the beginning, the beam-squints motivated measurements in an anechoic chamber to ensure a perfect LOS scenario without any possible reflections. Consequently, the preferred beam directions can exactly be specified. Fig. 2 shows the receiver of the multiple-antenna demonstrator in the anechoic chamber mounted on an antenna rotator. After the occurring phase errors were pinpointed in the LO paths of the antenna elements, the specific phase distortions in each Tx and Rx antenna branch must be determined with the goal to simply derotate the relative phase differences between the antennas. Therefore, two different measurement set-ups were built. At first, the relative phase differences at the receiver $\Delta\varphi_{\mathrm{R},i}$ must be determined via channel sounding procedures. Therefore, data samples based on a complex exponential with frequency $f_{\mathrm{e}} = 49$ kHz are transmitted via a single Tx antenna and received with all possible Rx antennas (SIMO). After removing the time-invariant DC baseband component coming from the self-mixed LO signal, the relative phase differences between the antennas compared to a reference antenna can directly be obtained after separately taking the mean of the almost constant phases by

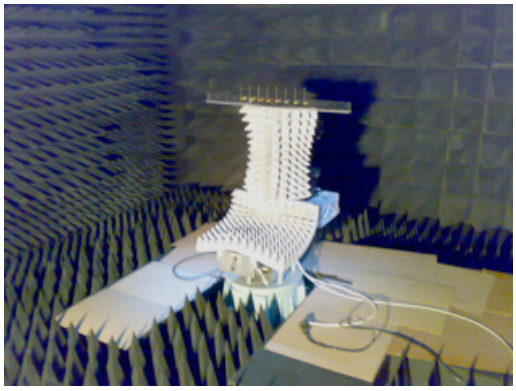

Fig. 2. Multiple-Antenna Demonstrator MASI in anechoic chamber

$$\Delta\varphi_{\mathrm{R},i} = \varphi_{\mathrm{R},i} - \varphi_{\mathrm{R,ref}} \ , \tag{11}$$

where $\varphi_{\mathrm{R},i}$ denotes the measured mean phase at receive antenna i. During all measurements the reference antenna was set to be the first antenna such that $\varphi_{\mathrm{R,ref}} = \varphi_{\mathrm{R},1}$. This leads to the correction matrix

$$\mathbf{\Phi}_{\mathrm{c}}^{(\mathrm{Rx})} = \mathrm{diag}\left\{\left[1, \mathrm{e}^{(-j\Delta\varphi_{R,2})},\ldots,\mathrm{e}^{\left(-j\Delta\varphi_{R,N_R}\right)}\right]\right\} \tag{12}$$

which accounts for the relative phase deviations of the different Rx LO amplifiers.

The relative phase differences at the transmitter side cannot be obtained directly. For that purpose, in a single frame time-multiplexed complex exponentials with fixed length and equal frequency of $f_{\mathrm{e}} = 190$ kHz are transmitted repeatedly over multiple antennas and received with a single Rx antenna (MISO). An example of the real part of such a transmit signal for four Tx antennas is shown in Fig. 3. After removing the DC offset again, the beginning of the transmitted frame has to be detected in the MASI Rx memory and the frequency offset is corrected. The repeated exponentials corresponding to a Tx antenna are assembled and the time-dependent phase difference according to the reference antenna is calculated similarly to (11). Additional low-pass filtering smoothes the curves and small phase jumps are ignored for simplicity. The mean of the relative phase differences results in

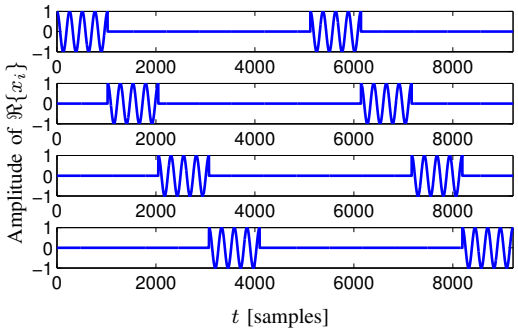

Fig. 3. Exemplary Tx signal (real part) for 4 transmit antennas of the applied MISO channel sounding to measure the relative phases of the Tx LO paths

a Tx correction matrix $\mathbf{\Phi}_{\mathrm{c}}^{(\mathrm{Tx})}$ according to (12). Both correction matrices are stored once to enable off-line compensation even in real-world scenarios outside the anechoic chamber. The correction of the Tx and Rx phase deviations can then be done sequentially at the receiver.

Mathematically, this can be expressed as

$$\begin{aligned}\hat{\mathbf{H}} &= \left(\mathbf{\Phi}_{\mathrm{c}}^{(\mathrm{Tx})}\left(\mathbf{\Phi}_{\mathrm{c}}^{(\mathrm{Rx})}\tilde{\mathbf{H}}\right)^{T}\right)^{T} \\ &= \left(\mathbf{\Phi}_{\mathrm{c}}^{(\mathrm{Tx})}\mathbf{\Phi}_{\mathrm{T}}^{T}\mathbf{H}^{T}\mathbf{\Phi}_{\mathrm{ref}}^{(\mathrm{Rx})T}\right)^{T} \\ &= \mathbf{\Phi}_{\mathrm{ref}}^{(\mathrm{Rx})}\mathbf{H}\mathbf{\Phi}_{\mathrm{ref}}^{(\mathrm{Tx})} \,. \end{aligned} \tag{13}$$

The matrices $\mathbf{\Phi}_{\mathrm{ref}}^{(\mathrm{Tx})} = \exp\left(j\varphi_{\mathrm{T,ref}}\right)\mathbf{I}_{N_{\mathrm{T}}}$ and $\mathbf{\Phi}_{\mathrm{ref}}^{(\mathrm{Rx})} = \exp\left(j\varphi_{\mathrm{R,ref}}\right)\mathbf{I}_{N_{\mathrm{R}}}$ describe the remaining phase errors due to the assumption in (11). The identity matrix structure of both matrices weighted with constant terms causes a common constant overall phase error such that

$$\hat{\mathbf{H}} = \mathrm{e}^{(j(\varphi_{\mathrm{T,ref}}+\varphi_{\mathrm{R,ref}}))}\mathbf{H} \,. \tag{14}$$

This phase error cannot be removed in the calibration process. For the purpose of investigating the array factors in (7) this phase error vanishes due to the definitions in (5) and (6).

V. Measurement Results

To compare the results obtained in [4] with the calibrated system described in Section IV we set the number of transmit and receive antennas to $N_{\mathrm{T}} = N_{\mathrm{R}} = 4$. The site distance of both ULAs with antenna spacing $d = \lambda/2$ in an ordinary office room is set to $s \approx 5$ m and their alignment relates to a broadside orientation with rotation angle $\alpha = 0°$. The carrier frequency is $f_{\mathrm{c}} = 2.44$ GHz with a sampling frequency of 50 MHz and an oversampling factor of $w = 8$. With this set-up a channel with a strong LOS component, i.e., a low-rank channel is expected. To estimate this narrow-band channel time-multiplexed polyphase sequences are transmitted. Fig. 4 shows the eigenbeams measured in this scenario with and without calibration of the relative phase deviations.

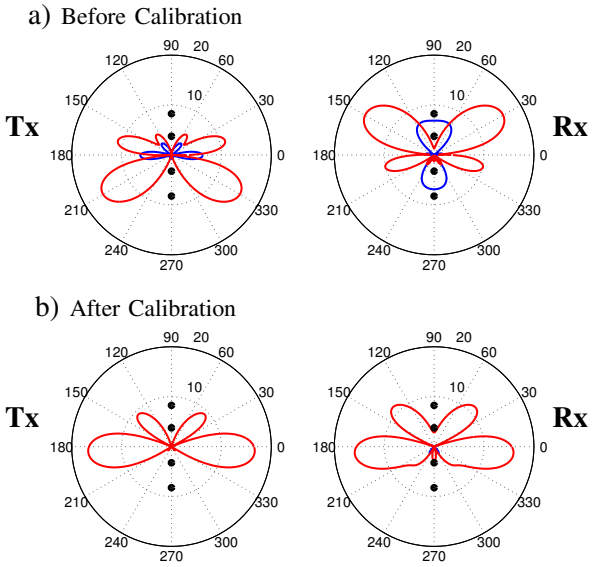

Fig. 4. Polar plots of eigenbeams at TX and RX of a 4×4 MIMO system with a strong LOS component a) before and b) after calibration of phase deviations

In Fig. 4a) the polar plots of the eigenbeams without calibration show a squint of the strongest eigenbeam lobes of around 30° at both the Tx and the Rx end. A smaller second eigenmode of the channel (*blue* color) is observed even in this strong LOS scenario. Although it was shown that the rank of the channel cannot change due to the definitions in (9) and (10), multiple eigenmodes may still result for small arrays distances (cf. [4]). In contrast, only one dominant eigenmode could be obtained during the measurements for the calibrated system in Fig. 4b). More important, the plot indicates that the beam-squints could be removed almost completely due to the implemented off-line compensation of the LO phase distortions.

The DOAs and DODs of the preferred directions can usually be obtained by using signal subspace algorithms like MUSIC [9], which are similar in finding the maximum array factor of the Tx and Rx array, respectively. To confirm the effectiveness of the compensation of the LO phase distortions, a series of measurements with a rotating receive array from broadside to endfire orientation ($\alpha \in [0°, \ldots, 90°]$) and the same parameters was carried out in the anechoic chamber.

The result can be seen in Fig. 5. Obviously, the

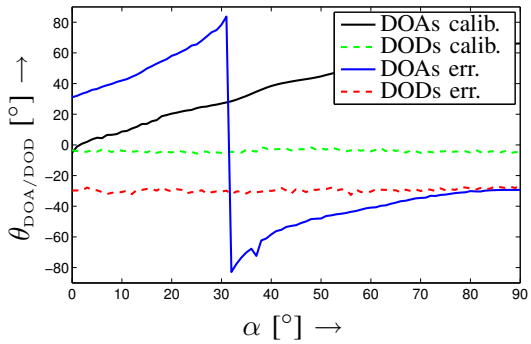

Fig. 5. DOA's and DOD's of the erroneous and the calibrated 4×4 system versus the receive array rotation angle α

DOAs and DODs of the erroneous system exhibit a constant phase discrepancy of around 30° as aforementioned. Due to the steady angle of the Tx array, the DODs remain constant for all α. After calibration the DOD is corrected to the zero degree direction of the Rx array. The rotating Rx array, however, causes an almost linear developing of the DOAs, as expected also starting from zero degree direction.

Additional measurement results in a NLOS scenario are depicted in Fig. 6, where the transmitter and the receiver are aligned in endfire position and approximately 3 m laterally shifted such that a wall circumvents the propagation of a LOS component at around 31°. Multiple reflections become possible due to located metal cupboards on the institute floors. In this situation at least three transmission

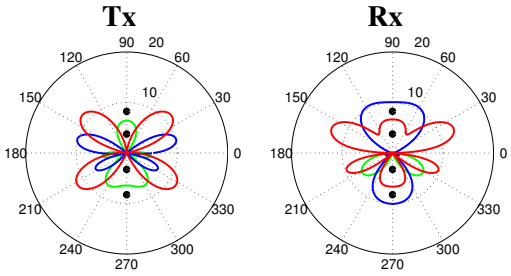

Fig. 6. Polar plots of (calibrated) eigenbeams at TX and RX of a 4×4 MIMO System with no LOS component

modes of the channel are visible in the eigenbeam plot. Now, the strongest eigenbeams (*red* color) are still aiming at the position of the opposed array, but have less power compared to the LOS scenario. Seemingly, the wall only attenuates the signal but cannot totally prevent propagation. The other eigenbeams have similar powers in other directions such that adaptive procedures are feasible in such conditions.

VI. Conclusion

In our contribution we presented eigenbeam measurement results with our multiple-antenna demonstrator MASI and an off-line phase calibration of the relative phase deviations resulting from different LO amplifiers in the MASI system. The calibrated system no longer exhibits severe beam-squints in the geometrical interpretation of the array factor gains corresponding to the existing eigenbeams. Thus, an evaluation of existing propagation scenarios is possible.

In the future, additional measurement and calibration approaches are planned to assess the influence of imperfect hardware components on the channel reciprocity.

Acknowledgements

The authors like to thank Dipl.-Ing H. Masemann for the preparations and the support during the measurements and the Department of RF & Microwave Engineering at the University of Bremen for providing the anechoic chamber and measurement equipment.

References

[1] 3GPP TSG RAN: "Evolved Universal Terrestrial Radio Access (E-UTRA) and Evolved Universal Terrestrial Radio Access Network (E-UTRAN); Overall description; Stage 2", *Technical Spec.*, TS 36.300 V8.3.0, Dec. 2007.

[2] J. Rinas, R. Seeger, L. Brötje, S. Vogeler, T. Haase and K.-D. Kammeyer, "A Multiple-Antenna System for ISM-Band Transmission", *EURASIP Journal on Applied Signal Processing - Special Issue on Advances in Smart Antennas*, Volume 2004, No. 9, pp. 1407-1419, Aug. 2004.

[3] M. Guillaud, D.T.M. Slock and R. Knopp, "A Practical Method for Wireless Channel Reciprocity Exploitation through Relative Calibration", *8th International Symp. on Signal Proc. and Its Applications (ISSPA 05)*, Vol. 1, pp. 403-406, Sydney, Australia, Aug. 28-31, 2005.

[4] H. Paul, "Implementierung von adaptiven Mehrantennen-Übertragungsverfahren", Diploma Thesis (In German), University of Bremen, Germany, Dec. 2006.

[5] C. Michalke, M. Stege, F. Schäfer, and G. Fettweis, *"Efficient Tracking of Eigenspaces and its Application to Eigenbeamforming"*, in Proc. of IEEE PIMRC, Vol. 3, pp. 2847-2851, Beijing, China, Sep. 7-10, 2003.

[6] J.C. Liberti, Jr. and T.S. Rappaport, *Smart Antennas For Wireless Communications: IS-95 and Third Generation CDMA Applications*, Prentice Hall, Upper Saddle River, New Jersey, USA, 1999.

[7] J. Rinas and K.-D. Kammeyer, "MIMO Measurements of Communication Signals and Application of Blind Source Separation", *Proc. of IEEE Intern. Symposium on Signal Processing and Information Technology (ISSPIT '03)*, pp. 94-97, Darmstadt, Germany, Dec. 14-17, 2003.

[8] R. Seeger, L. Brötje and K.-D. Kammeyer, "A MIMO Hardware Demonstrator: Application of Space-Time Block Codes", *Proc. of IEEE Intern. Symposium on Signal Processing and Information Technology (ISSPIT '03)*, pp. 98-101, Darmstadt, Germany, Dec. 14-17, 2003.

[9] N.E. Hurt, "Maximum Likelihood Estimation and MUSIC in Array Localization Signal Processing: A Review", *Multidimensional Systems and Signal Processing*, Vol. 1, No. 3, pp. 279-325, 1990.